

Charge-ordering, commensurability and metallicity in the phase diagram of layered Na_xCoO_2 .

Maw Lin Foo¹, Yayu Wang², Satoshi Watauchi^{1†}, H. W. Zandbergen^{3,4}, Tao He⁵, R. J. Cava^{1,3}, and N. P. Ong^{2,3}

¹*Department of Chemistry, ²Department of Physics,*

³*Princeton Materials Institute, Princeton University, New Jersey 08544, U.S.A.*

⁴*National Centre for HREM, Laboratory of Materials Science, Delft University of Technology, The Netherlands*

⁵*DuPont Central Research and Development Experimental Station, Wilmington, Delaware 19880, U.S.A.*

(Dated: February 8, 2020)

The phase diagram of non-hydrated Na_xCoO_2 has been determined by changing the Na content x using a series of chemical reactions. We find that as x increases from 0.3, the ground state goes from a paramagnetic metal to a charge-ordered insulator (at $x = \frac{1}{2}$) to a ‘Curie-Weiss metal’ (around 0.70), and finally to a weak-moment magnetically ordered state ($x > 0.75$). The unusual properties of the state at $\frac{1}{2}$ (including particle-hole symmetry at low T and enhanced thermal conductivity) are described. Implications for the superconducting phase (when water is intercalated) are discussed.

Research on oxide conductors has uncovered a spate of novel electronic behavior engendered by strong interaction between the charge carriers. In addition to unconventional superconductivity, the strong interaction leads to charge- and spin-ordered states as well as anomalous properties that are poorly described by standard transport theory [1, 2]. Recently, attention has focussed on Na_xCoO_2 , which exhibits an unusually large thermopower (for $x \sim \frac{2}{3}$) [3]. Despite being a good metal, Na_xCoO_2 shows a Curie-Weiss susceptibility consistent with local moments [4, 5]. The large thermopower has been related to the spin entropy carried by holes (Co^{4+} sites) hopping on a triangular lattice [4]. When intercalated with water, $\text{Na}_x\text{CoO}_2 \cdot y\text{H}_2\text{O}$ becomes superconducting at 4 K [6] in the doping region $\frac{1}{4} < x < \frac{1}{3}$ [7, 8, 9]. We report the phase diagram of non-hydrated Na_xCoO_2 for $0.31 < x < 0.75$. We uncover 2 distinct metallic states separated by an insulating state that is stabilized at $x = \frac{1}{2}$ by charge ordering of the holes and the Na ions. We identify details specific to the triangular lattice, especially in the metallic state from which the superconducting composition evolves.

A characteristic of non-hydrated Na_xCoO_2 is the sensitivity of the electronic states to slight changes in x . Starting with powder or single-crystal samples $x \sim 0.75$, we prepared a series of samples doped at varying x by specific chemical deintercalation of Na (Fig. 1, caption). Considerable care was taken to determine x reliably in each crystal investigated. By combining powder X-ray diffraction (XRD) and inductively-coupled plasma analysis (ICP) experiments, we measured accurately the variation of the c -axis lattice parameter vs. x (Fig. 1C). Powders of $\text{Na}_{0.77}\text{CoO}_2$ were made by solid-state reaction of stoichiometric amounts of Na_2CO_3 and Co_3O_4 in oxygen at 800 C. Sodium de-intercalation was then carried out by treatment of samples in solutions obtained by dissolving I_2 (0.2 M, 0.04 M) or Br_2 (1.0 M) in acetonitrile. After magnetic stirring for five days at ambient temperature, they were washed with copious amounts of acetonitrile and multiple samples were tested by the ICP-AES method to determine Na content. Unit-cell parameters were determined by powder XRD with internal Si stan-

dards. For the transport studies, we first grew a boule (with $x = 0.75$) in an optical furnace by the floating-zone technique. Crystals cleaved from the boule ($1.5 \text{ mm} \times 2 \text{ mm} \times 0.2 \text{ mm}$) were immersed in solutions of I_2 , Br_2 in acetonitrile or NaClO_3 in water for up to 2 weeks to deintercalate sodium. Excellent uniformity of Na content for these deintercalated crystals as verified by powder XRD, and by EDX analysis in the TEM.

Figure 1A shows the systematic variation of the magnetic susceptibility χ with x . Previous work shows that for $x \sim \frac{2}{3}$, χ vs. T follows the Curie-Weiss law $\chi = C/(T + \theta)$ with $\theta \sim 70 \text{ K}$. As x is increased slightly to 0.75, we find that χ is slightly rounded below 20 K, consistent with the appearance of a weak magnetization M ($\sim 0.03 \mu_B$ per Co with μ_B the Bohr magneton). A spin-density-wave (SDW) state at 0.75 has been suggested [10, 11]. The Curie-Weiss divergence in χ is systematically reduced with decreasing x until it is virtually suppressed at $\frac{1}{2}$. Close inspection of χ at $\frac{1}{2}$ reveals the existence of 2 sharp cusps at $T_{c1} = 88 \text{ K}$ and $T_{c2} = 53 \text{ K}$ (arrows). These 2 transitions are seen only if x is close to $\frac{1}{2}$. Below T_{c1} and T_{c2} , χ remains independent of the magnetic field H , so these are not transitions into magnetically ordered states. Finally, in the crystal with $x = 0.31$, χ is relatively featureless, although still quite large compared with the Pauli susceptibility in conventional metals.

In contrast with the smooth evolution of χ vs. x , the in-plane resistivity ρ shows a dramatic change in behavior across $x = \frac{1}{2}$ (Fig. 1B). At large x (0.68-0.75), ρ is metallic [3, 4, 10]. At $x = 0.75$, the shoulder near 20 K reflects the onset of weak magnetic order [11]. No magnetic ordering is observed for crystals in the Curie-Weiss state (0.68, 0.71), while ρ shows a T -linear behaviour at low T . In contrast to these metallic states, insulating behaviour abruptly appears at $x = \frac{1}{2}$ (note change in scale). Initially, ρ increases gradually as T falls towards T_{c1} and T_{c2} , where it exhibits weak anomalies. Below T_{c2} , however, ρ rises rapidly to reach $\sim 20 \text{ m}\Omega\text{cm}$ at 4 K. This insulating state is confined to a narrow interval in x . At the lower doping $x = 0.31$, we recover metallic behavior. Below 30 K, ρ follows a T^2 behavior and falls

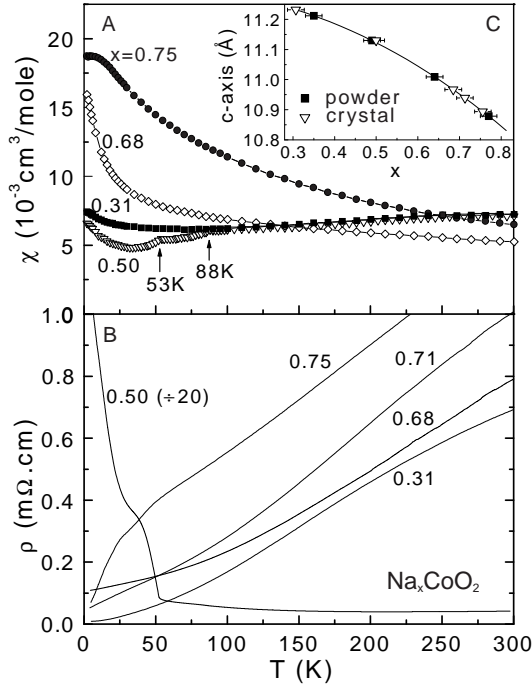


FIG. 1: The susceptibility χ (A) and in-plane resistivity ρ (B) of single crystals of Na_xCoO_2 with x determined by ICP (C). In Panel A, χ is measured in an in-plane field $H = 5$ T ($\mathbf{H} \perp \hat{\mathbf{c}}$). In the crystal with $x = 0.75$, χ fits the Curie-Weiss form $\chi = C/(T + \theta)$ (with $\theta \sim 150$ K and $C = 2.81 \text{ cm}^3\text{K}/\text{mole}$). For $x = 0.5$, sharp transitions are observed at T_{c1} and T_{c2} (arrows). Panel B shows the T dependence of ρ at selected x . Insulating behavior is observed at $x = 0.5$ (data displayed at lower scale) in contrast to metallic behavior in the rest. At low T , ρ is T -linear for $x = 0.71$ but varies as T^2 for $x = 0.3$. In Panel C, the c -axis lattice parameter measured by XRD is plotted against the Na content x fixed by ICP in powder samples.

to a small value ($9 \mu\Omega\text{cm}$) about 5 times lower than at $x = 0.71$.

The results from χ and ρ imply the phase diagram displayed in Fig. 2. The dominant feature in the T - x plane is the narrow insulating state at $x = \frac{1}{2}$ which separates two distinct metallic states. Below $\frac{1}{2}$, we have a ‘paramagnetic metal’ with high conductivity whereas, above $\frac{1}{2}$, we have a ‘Curie-Weiss’ metallic state in which a T -linear ρ [4] coexists with a χ that is Curie-Weiss like [4, 5].

What is the nature of the insulating state at $x = \frac{1}{2}$? An important feature specific to this state is revealed by electron-diffraction studies (Fig. 2B). Even at 300 K, the Na ions at $x = \frac{1}{2}$ order as a superstructure with lattice vectors $a\sqrt{3}\hat{\mathbf{x}}$ and $2a\hat{\mathbf{y}}$ in the basal plane with a the hexagonal lattice parameter. By contrast, at other doping levels, the superstructure Bragg spots are either much weaker or absent.

The long-range nature of the Na superstructure is brought out clearly by the thermal conductivity κ mea-

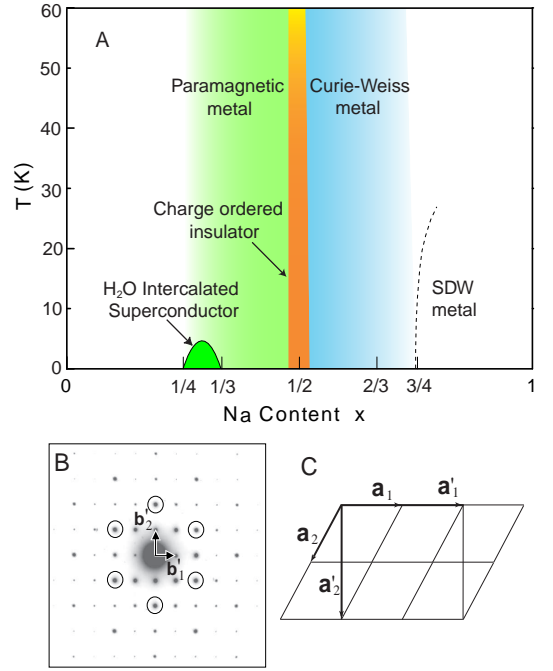


FIG. 2: The phase diagram of non-hydrated Na_xCoO_2 (A), electron diffraction pattern of a crystal with $x = \frac{1}{2}$ (B) and the Na superstructure lattice (C). In Panel A, the charge-ordered insulating state at $\frac{1}{2}$ is sandwiched between the paramagnetic metal at 0.3 and the Curie-Weiss metallic state at 0.65-0.75. The superconducting state is obtained on intercalation with H_2O [6, 7]. In Panel B, the diffraction pattern is taken along [001] with 200 kV electrons in a Phillips CM200 electron microscope. Bragg spots of the hexagonal lattice are encircled. The spots located at $n_1\mathbf{b}'_1 + n_2\mathbf{b}'_2$ correspond to the supercell with lattice vectors \mathbf{a}'_1 and \mathbf{a}'_2 drawn in Panel C.

sured parallel to the layers (in layered oxides, κ is dominated by the phonons). Because phonons are strongly scattered by disorder in the Na sublattice, we expect the phonon mean-free-path ℓ_{ph} to be much longer at $\frac{1}{2}$ than at neighboring x values. This is strikingly confirmed by the curves of κ vs. T (Fig. 3). In the metallic samples ($x = 0.31$ and 0.71), κ is only weakly T dependent and relatively small at all T . However, in the crystal with $x = \frac{1}{2}$, it rises steeply below T_{c2} to an exceptionally high value (300 W/mK) that is observed only in a handful of insulators like quartz and diamond. Both the diffraction and κ results provide strong evidence that, in sharp contrast with the metallic states, the Na ions at $x = \frac{1}{2}$ order with very long range correlation even at 300 K.

Further insight into the insulating state is provided by the Hall coefficient R_H (Figs. 3A and C). At $\frac{1}{2}$, we find that, above 200 K, R_H is hole-like with a T -independent value equivalent to a Hall density $1/eR_H = 1.8 \times 10^{21} \text{ cm}^{-3}$. (In metallic samples, however, R_H is T dependent; see below). Near T_{c1} , R_H rises to a weak maximum and then plunges to large negative values. Below T_{c2} , it increases dramatically in magnitude to a peak value 250 times greater than its magnitude above 200

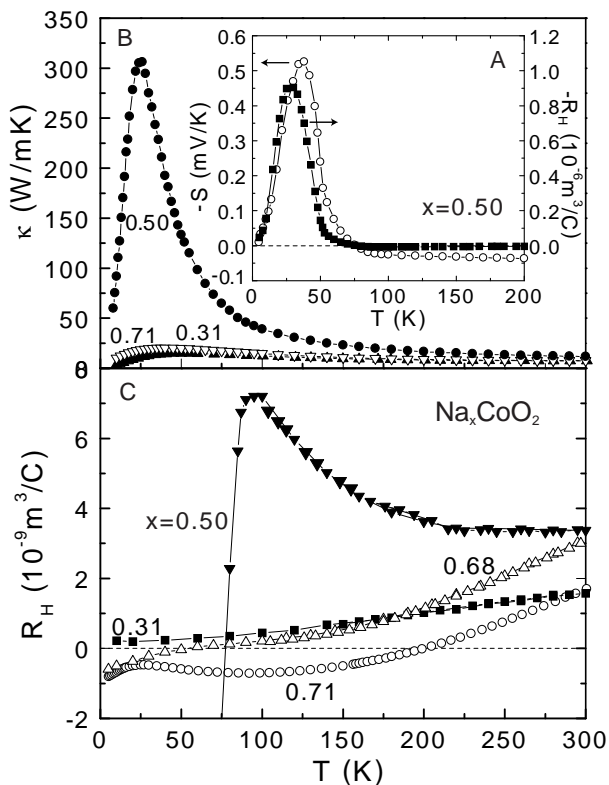


FIG. 3: The thermopower S and the Hall coefficient R_H in Na_xCoO_2 for $x = \frac{1}{2}$ (A), and plots of the in-plane thermal conductivity κ (B), and R_H (C) for several values of x . In Panel A, both $|S|$ and $|R_H|$ begin to increase steeply just below T_{c2} (88 K) and attain maxima at 40 and 30 K, respectively (note $-S$ and $-R_H$ are plotted). Below the peak values, they fall towards zero as $T \rightarrow 0$, consistent with a particle-hole symmetric state. In Panel B, κ at $x = \frac{1}{2}$ rises to a very large peak value comparable to that of quartz, whereas it remains small at all other x . Panel C shows that the curve of R_H vs. T at $x = 0.50$ is qualitatively different from all other x values. In the metallic samples, R_H increases with T , consistent with strongly interacting carriers hopping on a triangular lattice.

K. The giant increase in $|R_H|$ implies that the itinerant carrier density n decreases by ~ 2 orders of magnitude. The profile of the in-plane thermopower S is qualitatively similar. S changes sign near T_{c1} , and attains a large negative peak below T_{c2} . However, the relative increase in magnitude (~ 20) is smaller.

The behavior of R_H at low T reveals an unusual feature of the insulating state. $|R_H|$ falls steeply towards zero as $T \rightarrow 0$. This contrasts with the usual behavior in semiconductors where it diverges as $1/n$ (as $n \rightarrow 0$). In general, we have $R_H = \sigma_H/H\sigma^2$, with σ_H the Hall conductivity and $\sigma = 1/\rho$ the conductivity. The decrease of R_H to zero as $T \rightarrow 0$ implies that σ_H must vanish faster than the rate at which ρ^2 is increasing. The vanishing of Hall current at low T implies that the charge excitations exhibit strict particle-hole symmetry. They are neither hole-like nor electron-like in their response to the applied field.

Previous transport [4, 12], magnetic [5], and angle-resolved photoemission, (ARPES) [13] experiments point to the conclusion that strong correlation is essential for understanding the electronic properties of Na_xCoO_2 . On the triangular lattice in the CoO_2 layer, a fraction $(1-x)$ of the sites are occupied by itinerant spin- $\frac{1}{2}$ holes (Co^{4+}) hopping in a diamagnetic background of Co^{3+} ions [4]. The hopping amplitude t for $x \sim \frac{2}{3}$ measured by ARPES [13] is unusually small ($t \sim 10$ meV). Recently, several groups have applied the tJ Hamiltonian to Na_xCoO_2 [14, 15, 16, 17]. The derived phase diagram is strongly informed by the classical lattice-gas model which predicts that, on the triangular lattice, the electrons (holes) crystallize into a $\sqrt{3} \times \sqrt{3}$ structure at $x = \frac{1}{3}$ ($\frac{2}{3}$) [17]. However, at $\frac{1}{2}$, commensurability effects are weakest and charge ordering is not favored. Hence the observed insulating state is unexpected.

To account for the insulating state, we propose that it is critical to include the interaction between the charge carriers and the Na ions. Although they occupy separate layers, their mutual interaction is strong enough to determine the electronic states. For either charge species alone on the triangular lattice at , the liquid state seems to be more stable at finite temperature. However, if both populations are present, density fluctuations in one will strongly influence the other. At $\frac{1}{2}$, the density of states of the carriers is sharply peaked. Hence the carriers respond strongly to potential fluctuations created by density modulations in the Na layer. The incipient localization of the holes is evident at 300 K as indicated by the weakly rising ρ (Fig. 1B). In turn, as the amplitude of the hole-density modulation grows, it becomes more favorable energetically for the Na ions to order. The strong coupling leads to a steep increase in both modulation amplitudes until a transition occurs in which the carriers condense into an insulating charge-ordered state. We point out that the particle-hole symmetry observed at low T supports our argument that the insulating state is tied to the singular point at $x = \frac{1}{2}$ on the triangular lattice. At this filling, a charge excitation is neither hole-like nor electron-like in its response to H .

It is interesting to compare the paramagnetic metal with the Curie-Weiss metal. As noted, at low T , σ is ~ 5 times higher in the former. The magnitude of R_H at 4 K indicates that the Hall density at 0.31 ($6.2 \times 10^{22}\text{cm}^{-3}$) is 3-5 times higher as well. In contrast to the T -linear behavior of ρ in the latter, the T^2 dependence at 0.31 is closer to Fermi-liquid behavior. Together, these observations imply that the paramagnetic metal is closer to a conventional metallic state than the state at 0.71. The larger n leads to a proportionately higher σ and better screening of the carriers. Nonetheless, the behavior of R_H at high T shares a common pattern in both metallic states (Fig. 3C). R_H increases monotonically with T over a broad range of T [12]. According to Ref. [15], this is characteristic of interacting electrons hopping on a triangular lattice. The T -linear increase is most pronounced at 0.71 but decreases in slope as x decreases to

0.31. In the latter there is also a slight decrease in slope at high T . To the extent that the anomalous T dependence of R_H reflects strong correlation on the triangular lattice, we infer that correlations are still present at 0.31, although weakened.

Finally, we remark that the superconducting state produced by intercalation with H_2O evolves from the paramagnetic metal which is separated from the Curie-Weiss state by the charge-ordered insulator. It is unlikely that antiferromagnetic correlations, so apparent at $x \sim \frac{2}{3}$, play a role in the superconducting state. Moreover, in the paramagnetic metal, we have not observed any evidence for $\sqrt{3} \times \sqrt{3}$ charge ordering, nor any evidence for a ferromagnetic instability. The large carrier density

($6.2 \times 10^{22} \text{cm}^{-3}$) implies that the superfluid density is comparable to that in low- T_c superconductors (and larger by 20 than the value in overdoped cuprates). These findings should place hard experimental constraints on theories of the superconducting mechanism.

We thank Thomas S. Connell for performing the ICP-AES analysis, and acknowledge support by a MR-SEC grant from the National Science Foundation (DMR 0213706).

†*Permanent address:* Center for Crystal Science and Technology, University of Yamanashi, 7 Miyamae, Kofu, Yamanashi 400-8511, Japan.

-
- [1] Y. Tokura, *Physics Today* **56**, 50 (2003).
 - [2] A. P. Mackenzie, and Y. Maeno, *Reviews of Modern Physics* **75**, 657 (2003).
 - [3] I. Terasaki, Y. Sasago, and K. Uchinokura, *Phys. Rev. B* **56**, 12685 (1997).
 - [4] Y. Wang, N. S. Rogado, R. J. Cava, and N. P. Ong, *Nature* **423**, 425 (2003).
 - [5] R. Ray, A. Ghoshray, K. Ghoshray, and S. Nakamura, *Phys. Rev. B* **59**, 9454 (1999).
 - [6] K. Takada *et al.*, *Nature* **422**, 53 (2003).
 - [7] R. E. Schaak, T. Klimczuk, M. L. Foo, and R. J. Cava, *Nature* **424**, 527 (2003).
 - [8] F. C. Chou, J. H. Cho, P. A. Lee, E. T. Abel, K. Matan, and Y. S. Lee, *cond-mat/0306659* (2003).
 - [9] R. Jin, B. C. Sales, P. Khalifah, and D. Mandrus, *cond-mat/0306066* (2003).
 - [10] T. Motohashi *et al.*, *Phys. Rev. B* **67**, 064406 (2003).
 - [11] J. Sugiyama *et al.* *cond-mat/0310516* (2003).
 - [12] Y. Wang, N. S. Rogado, R. J. Cava, and N. P. Ong, *cond-mat/0305455* (2003).
 - [13] M. Z. Hasan *et al.* *cond-mat/0308438* (2003).
 - [14] G. Baskaran, *Phys. Rev. Lett.* **91**, 097003 (2003).
 - [15] B. Kumar and B. S. Shastry, *cond-mat/0304210* (2003).
 - [16] Q. H. Wang, D. H. Lee, and P. A. Lee, *cond-mat/0304377* (2003).
 - [17] O. I. Motrunich and P. A. Lee, *cond-mat/0310387* (2003).